THE JOURNAL OF PHYSICAL CHEMISTRY Letters

Letter

pubs.acs.org/JPCL

Use of Nonequilibrium Work Methods to Compute Free Energy Differences Between Molecular Mechanical and Quantum Mechanical Representations of Molecular Systems

Phillip S. Hudson,[†] H. Lee Woodcock,*[,†] and Stefan Boresch*[,‡]

[†]Department of Chemistry, University of South Florida, 4202 East Fowler Avenue, CHE205, Tampa, Florida 33620-5250, United States

[‡]Department of Computational Biological Chemistry, Faculty of Chemistry, University of Vienna, Währingerstraße 17, A-1090 Vienna, Austria

Supporting Information

ABSTRACT: Carrying out free energy simulations (FES) using quantum mechanical (QM) Hamiltonians remains an attractive, albeit elusive goal. Renewed efforts in this area have focused on using "indirect" thermodynamic cycles to connect "low level" simulation results to "high level" free energies. The main obstacle to computing converged free energy results between molecular mechanical (MM) and QM ($\Delta A^{\mathrm{MM}\rightarrow\mathrm{QM}}$), as recently demonstrated by us and others, is differences in the so-called "stiff" degrees of freedom (e.g., bond stretching) between the respective energy surfaces. Herein, we demonstrate that this problem can be efficiently circumvented using nonequilibrium work (NEW) techniques, i.e., Jarzynski's and Crooks' equations. Initial applications of computing $\Delta A^{\mathrm{MM}\rightarrow\mathrm{QM}}_{\mathrm{NEW}}$, for blocked amino acids alanine and serine as well as to generate butane's potentials of mean force via the indirect QM/MM FES method, showed marked improvement over traditional FES approaches.

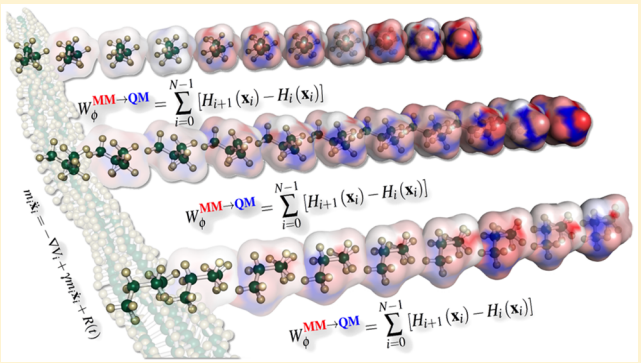

KEYWORDS: *QM/MM, nonequilibrium work techniques, free energy simulations*

Alchemical free energy simulations (FES) have become a standard tool of computational chemistry and biophysics. While classical force fields are sufficient in many cases, certain applications require the use of combined quantum chemical molecular mechanical (QM/MM) descriptions of interactions. The computational cost of using QM/MM Hamiltonians in free energy calculations, which typically require several simulations to obtain the final result of interest, is extremely high, even prohibitively so in many cases. To circumvent this limitation, Warshel and co-workers, as well as Gao and co-workers, introduced what is often referred to as the indirect approach to QM/MM FES.[1−6]

The thermodynamic cycle shown in Figure 1 is used to obtain the QM free energy difference between two states A and B in a stepwise fashion (i.e., $\Delta A^{\mathrm{QM}}_{\mathrm{A}\rightarrow\mathrm{B}}$). The connection between low and high level of theory, i.e., $\Delta A^{\mathrm{MM}\rightarrow\mathrm{QM}}$, is almost exclusively done with free energy perturbation (FEP)[7] with a few notable exceptions, such as linear response approximation (LRA).[8−10] However, it is well-known that using FEP to compute free energy differences in one step is reliable only if the two end states are very similar, which may not be the case for $\Delta A^{MM\rightarrow QM}$.[11] In fact, recent work by numerous groups denote this problem and highlight consequences that limit the applicability of QM/MM FES.[12−19]

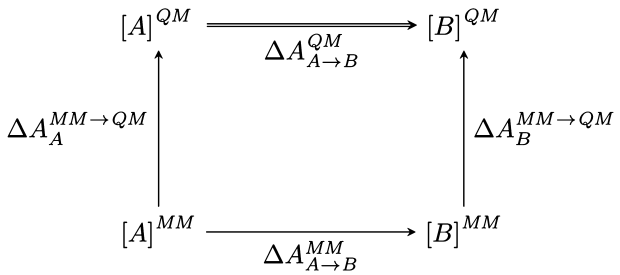

Figure 1. Thermodynamic cycle of the "indirect" scheme for QM/MM FES. $\Delta A^{\mathrm{QM}}_{\mathrm{A}\rightarrow\mathrm{B}} = -\Delta A^{\mathrm{MM}\rightarrow\mathrm{QM}}_{\mathrm{A}} + \Delta A^{\mathrm{MM}}_{\mathrm{A}\rightarrow\mathrm{B}} + \Delta A^{\mathrm{MM}\rightarrow\mathrm{QM}}_{\mathrm{B}}$. See Figure S1 for depiction of indirect scheme for potential of mean force generation.

We recently introduced the so-called QM Non-Boltzmann Bennett method (QM-NBB), which was shown to be a more robust alternative to FEP for computing $\Delta A^{\mathrm{QM}}_{\mathrm{A}\rightarrow\mathrm{B}}$ in Figure 1.[13] However, when attempting to compute solvation free energy differences for the N-acetyl-methylamide amino acids Alanine (Ala) and Serine (Ser) ("blocked" amino acids, often referred

Received: September 29, 2015
Accepted: November 5, 2015
Published: November 5, 2015

DOI: 10.1021/acs.jpclett.5b02164
J. Phys. Chem. Lett. 2015, 6, 4850−4856

Table 1. Free Energy Differences in kcal/mol for the Indicated Step between MM and SCC-DFTB (cf. Figure 1)[a]

	Ala						Ser					
	$\Delta A^{C22\rightarrow DFTB}$			$\Delta A^{C22(CMAP)\rightarrow DFTB3}$			$\Delta A^{C22\rightarrow DFTB}$			$\Delta A^{C22(CMAP)\rightarrow DFTB3}$		
method	ΔA	Hy	s	ΔA	Hy	s	ΔA	Hy	s	ΔA	Hy	s
FEP	−47.46	0.21	0.50	−55.31	1.29	1.00	−34.20	0.15	0.48	−45.72	0.55	1.02
JAR,FW100	−48.40	0.03	0.17	−54.98	0.02	0.12	−35.51	0.07	0.29	−46.71	0.15	0.43
JAR,FW500	−48.18	0.00	0.06	−54.80	0.01	0.08	−35.28	0.03	0.19	−46.74	0.12	0.40
BAR	−48.08	0.01	0.05	−54.83	0.00	0.03	−35.30	0.01	0.13	−46.71	0.02	0.17
CRO,100	−48.12	0.00	0.02	−54.82	0.00	0.02	−35.28	0.00	0.09	−46.72	0.02	0.16

[a]All Ala free energy differences are offset by +16 400 kcal/mol, all Ser results by +18 500 kcal/mol. The values in columns "ΔA" are the free energy difference obtained with the indicated method using all available 200 000 configurations; the exception being JAR,FW500 for which only 20 000 configurations were used. The Hy(steresis) column is an estimate of sample size hysteresis, $|\Delta A - 1/n \sum_i \Delta A_i|$, using n = 10 blocks of 20 000 (2000 for JAR,FW500) configurations to compute the ΔA_i. The standard deviation of the block mean $1/n \sum_i \Delta A_i$ is listed in column 's'.[26]

Table 2. Comparison of $\Delta A^{DFTB\rightarrow DFTB3}$ Generated Directly Using BAR (See Table S1) and $\Delta A^{DFTB\rightarrow DFTB3}_{cycle}$(= $-\Delta A^{C22\rightarrow DFTB} + \Delta A^{C22\rightarrow C22(CMAP)} + \Delta A^{C22(CMAP)\rightarrow DFTB3}$) Computed via the Indirect Approach Using the Thermodynamic Cycle Depicted in Figure 1 and the Data from Tables 1 and S1[a]

	Ala			Ser		
	$\Delta A^{DFTB\rightarrow DFTB3}_{cycle}$	s	ϵ_{cycle}	$\Delta A^{DFTB\rightarrow DFTB3}_{cycle}$	s	ϵ_{cycle}
FEP	−8.43	1.12	−1.14	−12.27	1.13	−0.14
JAR,FW100	−7.16	0.21	0.13	−11.95	0.52	0.18
JAR,FW500	−7.20	0.10	0.09	−12.21	0.45	−0.08
BAR	−7.33	0.06	−0.04	−12.16	0.22	−0.03
CRO,100	−7.28	0.03	0.01	−12.19	0.19	−0.06

[a]The error estimate, s, is obtained by Gaussian error propagation from the individual standard deviations. The cycle closure error ϵ_{cycle} is the difference $\Delta A^{DFTB\rightarrow DFTB3}_{cycle} - \Delta A^{DFTB\rightarrow DFTB3}$; the reference results $\Delta A^{DFTB\rightarrow DFTB3}$, obtained directly, are −7.29 kcal/mol for Ala and −12.13 kcal/mol for Ser, respectively (see Table S1). All values are reported in kcal/mol.

to as alanine and serine "dipeptides"), we also encountered severe convergence problems even when utilizing the QM-NBB framework (unpublished). We attributed this failure to poor overlap, primarily caused by the "stiff" degrees of freedom (e.g., bond stretching terms) in accord with our own, and others' previous findings.[12−19]

The difficulties of obtaining converged $\Delta A^{MM\rightarrow QM}$ results have typically been addressed by changing how the "low level" ensemble is generated[10,20] or by excluding energy terms that are responsible for poor overlap (e.g., stiff degrees of freedom).[15,18,19] However, herein we investigate the use of more robust FES techniques to connect MM and QM(/MM) levels of theory, in particular the use of nonequilibrium-work (NEW) methods. Our efforts are focused on the use of nonequilibrium equivalents of FEP and Bennett's Acceptance Ratio (BAR), i.e., Jarzynski's (JAR) and Crooks' (CRO) equations, respectively.[21−23] In these approaches, the potential energy differences between two states, 0 and 1, are replaced by the nonequilibrium work carried out in (relatively) short switching simulations between the two states. For example, JAR has the same formalism as Zwanzig's equation and reduces to Zwanzig's result in the case of instantaneous switching. [Symbols in eq 1 have the usual meaning, k_B is Boltzmann's constant, T is the temperature, and the angular brackets denote averaging over multiple switching simulations. The subscript 0 indicates that the switching calculations are initiated from an equilibrium distribution sampled at state 0.]

$$\Delta A_{0\rightarrow 1} = -k_B T \ln \left\langle \exp\left[\frac{-W_{0\rightarrow 1}}{k_B T}\right]\right\rangle_0 \quad (1)$$

Crooks' equation (eq 19 of ref 23) is realized analogously by replacing forward (0 → 1) and backward (1 → 0) energy differences in BAR with the corresponding forward and backward nonequilibrium work values.

Interestingly, in traditional alchemical FES, these NEW methods are rarely used as there is little practical gain in efficiency.[24] However, we expect them to be well-suited for the specific problem of calculating $\Delta A^{MM\rightarrow QM}$. In this study, we investigate $\Delta A^{MM\rightarrow QM}$ descriptions of the dihedral rotation of butane and the $\Delta A^{MM\rightarrow SQM}$ of blocked amino acids, exactly those systems where we observed convergence failure not only with FEP (butane), but also with QM-NBB (Ala→Ser). [(S)QM refers to the use of either semiempirical QM (SQM; e.g., SCC-DFTB) or ab initio/DFT QM Hamiltonians.] In this initial study we focus on the gas phase; after all, if NEW methods cannot overcome, the documented problems from the stiff degrees of freedom arising in FEP and QM-NBB, their use in real world (S)QM/MM applications would be highly doubtful.

The central goal of this work is the calculation of converged values of $\Delta A^{MM\rightarrow (S)QM}$ (MM → SCC-DFTB for Ala/Ser and MM → QM for butane). For the first model systems (i.e., Ala/Ser), $\Delta A^{MM\rightarrow SQM}$ could be computed by two-sided methods (BAR, CRO) since sufficiently long simulations at the "high" level of theory were feasible. For all energetic transitions studied, the BAR and CRO results agree extremely well, strongly suggesting that results are truly converged.

Detailed results for the various methods used can be found in Table 1. [C22 = CHARMM22 protein force field, C22(CMAP) = C22 + backbone corrections,[25] DFTB = SCC-DFTB, and DFTB3 = SCC-DFTB with third order corrections. The mio-1−1 parameters were used for both DFTB and DFTB3.] For all four transitions, FEP does a poor job, deviating by at least 0.5 kcal/mol from the BAR and CRO results. In each FEP case, there is either a strong indication of sample size hysteresis,[26] as

DOI: 10.1021/acs.jpclett.5b02164
J. Phys. Chem. Lett. 2015, 6, 4850−4856

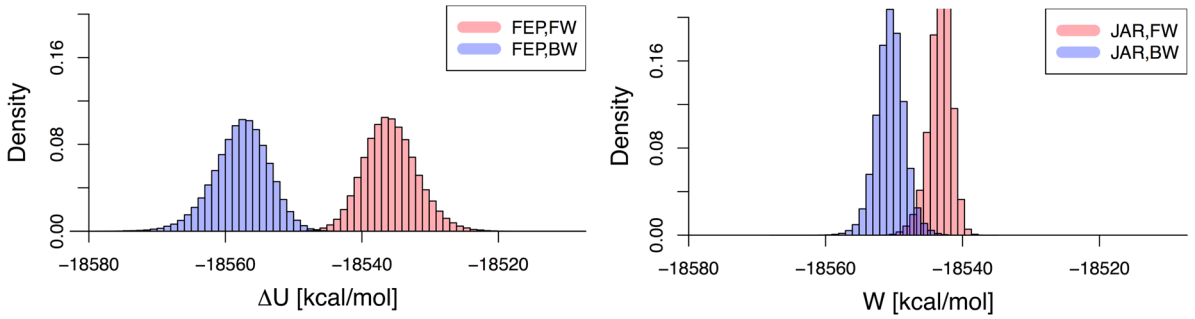

(a) ΔU Histograms (b) Work Histograms

Figure 2. Histograms of (a) forward potential energy differences $\Delta U^{\mathrm{FW|MM}} = U^{\mathrm{SQM|MM}} - U^{\mathrm{MM|MM}}$ versus that of the backward energy differences $-\Delta U^{\mathrm{BW|SQM}} = -(U^{\mathrm{MM|SQM}} - U^{\mathrm{SQM|SQM}})$ and (b) nonequilibrium forward work $W^{\mathrm{MM\to SQM|MM}}$ versus the nonequilibrium backward work $-W^{\mathrm{SQM\to MM|SQM}}$. The notation ...|*MM* and ...|*SQM* indicates that the energy differences/work values were computed for configurations sampled at the MM and SQM level of theory, respectively, where in the present case SQM stands for SCC-DFTB. Data shown for Ser, C22(CMAP) → SCC-DFTB.

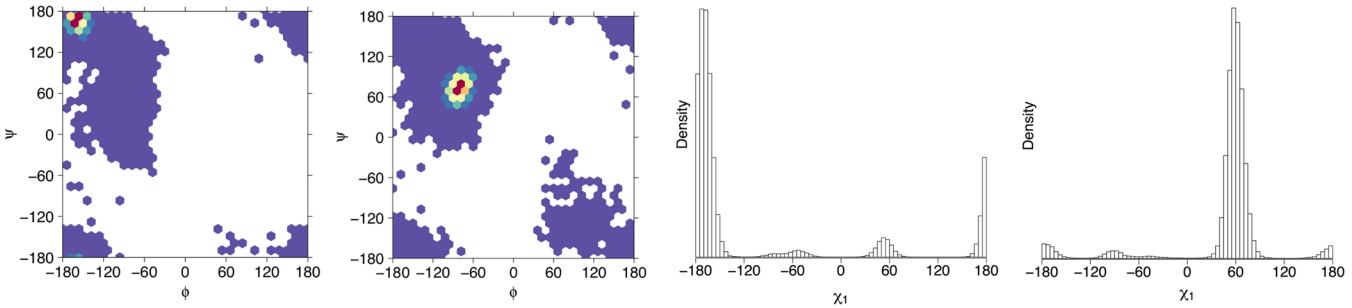

(a) C22(CMAP) (b) SCC-DFTB (c) C22(CMAP) (d) SCC-DFTB

Figure 3. Distribution of ϕ/ψ (a,b) and χ_1 (c,d) angles in Ser equilibrium simulations at the following levels of theory: (a) C22(CMAP), (b) SCC-DFTB, (c) C22(CMAP), and (d) SCC-DFTB.

seen by relatively large values in column "Hy", or a much larger standard deviation of the ΔA_i subset results about their mean (column 's'). By contrast, even with short switches, the NEW methods, such as JAR with 100 forward switching steps (FW100), considerably improve the agreement with BAR/CRO reference results compared to FEP. Interestingly, the longer switching simulations (JAR,FW500) improve agreement even more although only one tenth of the available configurations were used (i.e., 20 000 vs 200 000). Clearly, the convergence behavior of the JAR,FW100 and JAR,FW500 results suggest some potential for optimizing the protocols used in these NEW techniques.

The relatively small size of the systems and the use of SCC-DFTB made it possible to compute $\Delta A^{\mathrm{DFTB\to DFTB3}}$ directly via BAR; results are listed in Table S1. Clearly, in the present case, both $\Delta A^{\mathrm{DFTB\to DFTB3}}$ and $\Delta A^{\mathrm{C22\to C22(CMAP)}}$ could be calculated with extremely high precision. There are no indications of sample size hysteresis, and the overlap between forward and backward energy difference distributions was >90% at both the MM, as well as the SCC-DFTB level of theory. [When using BAR (Crooks' equation), we (i) check how many of the forward energy differences (work values) lie within the range of the negative backward energy differences (work values), and (ii) perform the same check for the backward differences versus the negative forward differences. The lower of the two values, expressed in percent of the total number of energy differences (work values) is our indicator of overlap.]

Thus, it follows that any differences between $\Delta A^{\mathrm{DFTB\to DFTB3}}$ computed directly versus indirectly, $\epsilon_{\mathrm{cycle}}$ (Table 2), are likely caused by problems computing $\Delta A^{\mathrm{MM\to SQM}}$. Pertinent results are summarized in Table 2. In the case of Ala, the cycle closing error for FEP is over 1.1 kcal/mol, whereas it is <0.2 kcal/mol for all other methods. For Ser, all methods have a low cycle closing error, but it is clear that FEP benefits from fortuitous error cancellation (i.e., both $\Delta A^{\mathrm{MM\to SQM}}$ are systematically wrong; see Table 1). Again, we see that the uncertainty, *s*, of FEP for the Ser cycle closing error is significantly higher than for all other methods used.

To illustrate why fast switching improves convergence, we plot the energy/work distributions generated from the respective FES (Figure 2). The histograms of the energy differences are quite broad, but still show some overlap. This overlap, albeit small, is sufficient for BAR to yield accurate results; however, for FEP the ensembles are far from ideal. In general, for any one sided method to yield converged results at least some of the configurations sampled at the initial state (MM) should be representative, i.e., low energy target state (SQM) conformations.[11] In the case of FEP (Figure 2), the almost nonexistent $\Delta U^{\mathrm{MM\to SQM}}$ overlap between the MM and the SQM ensembles indicates a large disparity of conformations at both states preventing convergence of $\Delta A^{\mathrm{MM\to SQM}}$ by FEP. In contrast, the irreversible work, $W^{\mathrm{MM\to SQM}}$ histograms (Figure 2b) are not only more narrowly distributed, but also give significant overlap between the MM and SQM ensembles, allowing for smooth convergence in computing $\Delta A^{\mathrm{MM\to SQM}}$.

While NEW simulations appear to easily circumvent the problem of "stiff" degrees of freedom when switching between MM and QM levels of theory, an equally troubling problem

DOI: 10.1021/acs.jpclett.5b02164
J. Phys. Chem. Lett. 2015, 6, 4850−4856

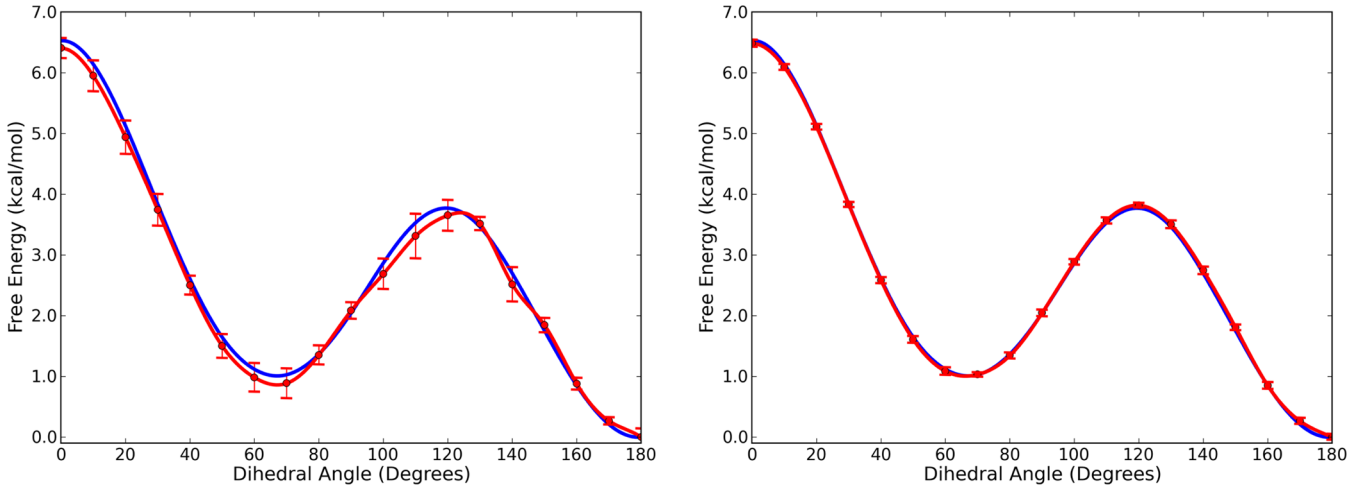

Figure 4. Butane potentials of mean force (PMF) generated (a) via traditional FEP ($\Delta A^{MM\rightarrow QM}$) using data from 1 ns MM simulations (100 000 points per dihedral step; red) compared to a reference PMF constructed with FEP ($\Delta A^{SCC-DFTB\rightarrow QM}$) using data obtained from 2 ns SCC-DFTB simulations (200 000 points per dihedral step; blue);[17] and (b) via Jarzynski's equation to obtain $\Delta A^{MM\rightarrow QM}$ using data from 1 ns MM simulations (1000 $W^{MM\rightarrow QM}$ values per dihedral step; red) compared to the aforementioned reference PMF (i.e., FEP(SCC-DFTB → QM); blue. Here QM means HF/6-31G*).

comes to light: the "soft" degrees of freedom. Therefore, we examined distributions of the pseudo backbone dihedral angles ϕ and ψ in the blocked amino acids, and for Ser also the χ_1 side chain dihedral angle (Figure 3). The resulting plots clearly indicate that significant conformational differences exist between the ensembles generated at MM (Figure 3a,c) and SCC-DFTB (Figure 3b,d). Furthermore, while the time scale for nonequilibrium switching is sufficient for the "stiff" degrees of freedom, the "soft" ones remain close to their initial MM values (Figures S2−S3). Thus, Figures 3, S2 and S3 may raise the question why the NEW simulations work, given the differences in conformational preferences between MM and SCC-DFTB. The key observation is that the MM simulations, as well as the switching simulations, *do* sample conformational space relevant at the SCC-DFTB level of theory, albeit rarely. Using NEW approaches, these few configurations are enough, since mismatches between the stiff degrees of freedom for these configurations were mostly removed during the switching simulations. By contrast, in the case of FEP, practically all configurations that are relevant in terms of conformational preferences will be unfavorable because of the stiff degrees of freedom differences. Nevertheless, it is easy to envision situations where the low level of theory will fail to sample conformational regions that are important at the high level of theory. In such cases, any treatment focusing exclusively on the stiff degrees of freedom is likely to fail.

Although the use of Crooks' equation is clearly the most attractive choice, this would be prohibitively expensive if the "high" level of theory was ab initio or DFT based (i.e., requiring long equilibrium MD simulations). Thus, for our initial test case (dihedral rotation of butane), we have focused on generating accurate potentials of mean force (PMF) using Jarzynski's one-sided method (Figure S1). A cursory glance at Figure 4a showcases the failure of FEP to produce meaningful $\Delta A^{MM\rightarrow QM}$ results for butane's PMF. Of particular concern is the relative extrema at 120° and 60° in which the standard deviations are larger than the free energy difference to the next consecutive step, implying a large level of sample size hysteresis. Results obtained using JAR,FW50 fast switching (Figure 4b), however, yield marked improvement over FEP between MM and HF/6-31G*; pathway RMSE 0.03 vs 0.13 kcal/mol, respectively. Some slight discrepancies observed in the NEW QM PMF are seen at the maxima, again, indicating that the soft, dihedral, degree of freedom is critical. Although QM-based NEW methods may be impractical to switch between states (e.g., along the reaction coordinate), the computational cost of generating butane's PMF via indirect FES (i.e., $\Delta A_{n^\circ}^{MM\rightarrow QM}$, n = 180,170,...,10,0) was ∼3/4 that of traditional indirect FEP. [The computational cost of FEP vs JAR,FW50 was determined based on total number of QM calculations per $\Delta A^{MM\rightarrow QM}$ (NEW: 1000 fast switches of 50 steps [QM force] each = 50 000; FEP: 100 000 QM single point energy calculations). Further, we estimate that a QM force (energy + gradient) will take approximately 1.5 times that of a QM single point. Thus, ∼ 75 000 (NEW) vs 100 000 (FEP).]

Our results clearly demonstrate that NEW methods make it possible to compute converged free energy differences $\Delta A^{MM\rightarrow QM}$ as required in indirect QM/MM FES approaches. During the (fast) switching simulations, the stiff degrees of freedom, which are now widely considered as the root cause of poor convergence in traditional FEP, can relax, leading to much improved convergence. The present study is an initial proof-of-concept; obviously, further work is needed to determine the most efficient protocol for use with QM/MM NEW approaches. Concerning the potentially significant computational costs, two aspects should be kept in mind. First, use of Jarzynski's equation, just as FEP, constitutes a postprocessing step, which can be parallelized very efficiently. Second, given that the use of NEW techniques is an exact approach, it can be used at least for model systems to gauge the correctness of alternative, faster methods. Finally, our results show that differences between low (e.g., MM) and high (e.g., QM) levels of theory are *not* restricted to the stiff degrees of freedom (e.g., bond stretching, angle bending); in fact, differences in conformational preferences may well prove to be the more daunting challenge when connecting levels of theory.

DOI: 10.1021/acs.jpclett.5b02164
J. Phys. Chem. Lett. 2015, 6, 4850−4856

METHODS

In this work, state 0 corresponds to a low level of theory (e.g., MM), whereas state 1 is the high level of theory (e.g., SCC-DFTB, QM). Using CHARMM, mixing MM and QM descriptions is possible via the MSCALE facility.[27,28] This allows combining of various "in house" features such as CHARMM's MM force field with a SCC-DFTB semiempirical Hamiltonian or CHARMM's QM/MM routines coupled with an external program (e.g., Q-Chem, GAMESS, etc.).[29−33]

Further, MSCALE supports the PERT free energy facility of CHARMM; thus, the degree of mixing between MM and QM is not only controllable, but can be modified continually through the course of a MD simulation as in slow-growth free energy simulations. Free energy differences obtained by slow-growth are in fact nonequilibrium work values. While in typical slow-growth calculations the control parameter λ is changed so slowly that the system is assumed to be almost at equilibrium, we deliberately used rather rapid switches and recover equilibrium free energy differences through Jarzynski's and Crooks' equation. The work between two steps of a switching simulation is accumulated according to

$$W(t+\delta t) = W(t) + H(\mathbf{r}(t+\delta t), \lambda(t+\delta t)) - H((\mathbf{r}(t+\delta t), \lambda(t)) \quad (2)$$

H is the Hamiltonian of the system, and $\mathbf{r}(t)$ denotes the state of the system. The switch is enforced by changing the control parameter $\lambda = \lambda(t)$ from $\lambda(0) = 0$ to $\lambda(t_{switch}) = 1$ over n_{switch} time steps for the full switching simulation, i.e., the switching time is given by $t_{switch} = n_{switch}\delta t$. The total nonequilibrium work $W_{0\to1}$ of eq 1 is the sum of the n_{switch} individual contributions given by eq 2. The switching simulations are started from coordinates/velocities saved during an equilibrium simulation in the canonical ensemble; the actual switch can then be carried out during dynamics in the microcanonical or canonical ensemble, including Langevin dynamics (LD).[24]

The free energy differences for the blocked amino acids, as shown in the cycle Figure 1 were computed based on extensive simulations of each state (i.e., level of theory), C22, C22(CMAP), DFTB, DFTB3. Excluding equilibration, a total of 200 million steps of LD for each state and amino acid were carried out. This consisted of two sets of LD simulations, each consisting of 100 million steps, started from different initial velocities. When using SCC-DFTB, a total of 20 simulations, each consisting of 10 million MD steps, started from different initial random velocities were carried out. Unless otherwise noted, the data generated during these individual simulations were treated as if obtained from a single, cumulative simulation. The time step in all simulations was 0.5 fs, and the friction coefficient was 5 ps^{-1} for all atoms. Coordinates and velocities were saved every 0.5 ps (1000 steps) by means of writing restart files (200 000 coordinate/velocity sets total). Neither cutoff nor switching and/or shifting functions were applied to the intramolecular nonbonded interactions. In all simulations, as well as fast switching calculations (see below), a center of mass restraint was applied to keep the molecule near the origin.

The coordinates saved during the production simulations were used to compute the free energy differences of interest (see Figure 1) by equilibrium methods (BAR, FEP). First, the coordinate information was used to compute the energy differences ΔU needed for FEP and BAR. All possible energy differences along the arrows in Figure 1, both in forward and backward directions, e.g., $\Delta U^{C22\to DFTB}$ based on coordinates saved during the C22 simulation, as well as $\Delta U^{DFTB\to C22}$ based on coordinates saved during the DFTB simulation were calculated.

Second, free energy differences $\Delta A^{MM\to SQM}$ along the vertical legs of the thermodynamic cycle Figure 1 were also computed by nonequilibrium methods. To do so, fast switching simulations were carried out to compute W of going from the MM to the SCC-DFTB Hamiltonian. The switches were carried out under identical conditions to those of the initial equilibrium simulations (i.e., those where the coordinate/velocity information was generated and saved). Switches were made linearly from the initial to final state using the MSCALE module of CHARMM. Fast switches over 100 steps of LD were carried out in both directions for all 200 000 restart files available, i.e., from MM to SCC-DFTB, as well as from SCC-DFTB to MM. In addition, fast switches over 500 LD steps were carried out in the MM to SCC-DFTB direction. Here, only every tenth restart file was used, i.e., only 20 000 switches were carried out. The NEW data were then used to compute $\Delta A^{MM\to SQM}$ using Jarzynski's equation as well as Crooks' equation.

To analyze our results for systematic and statistical errors, a simple test was carried out in a similar manner to analysis by Wood et al. of how FEP fails for disparate states.[26] Free energy differences were first computed using all available data; 200 000 data points in most cases, denoted ΔA^*. Then the full data set was divided into 10 sets, each containing 1/10 of the data, and the free energy was computed for each of the ten subsets (ΔA_i, i = 1,..., 10). For the two-sided methods (BAR, CRO), the subsets were comprised of both forward and backward data. We then computed $\langle \Delta A_i \rangle = 1/n \sum_i \Delta A_i$ for n = 10. If the FES are well converged, one should find $\Delta A^* \approx \langle \Delta A_i \rangle$. Any sizable deviations between ΔA^* and $\langle \Delta A_i \rangle$ indicates systematic errors due to sample size hysteresis.[26] For FEP and JAR, it was also helpful to monitor the cumulative average of ΔA for sudden jumps as an indication of sample size hysteresis. The 10 ΔA_i results were also used to compute a standard deviation about their mean, which again is an indicator of statistical error. The coordinates saved during the production simulations were further used to compute statistics about ϕ/ψ distributions, and, in the case of Ser, also statistics of the χ_1 distribution.

The potentials of mean force (PMF) for butane were obtained as follows. Simulations were carried out at an MM level with CHARMM General Force Field (CGenFF)[34] and with a 100 kcal mol^{-1} rad^{-2} harmonic restraint on the main "soft" degree of freedom, i.e., the C−C−C-C dihedral angle, at 10° increments between 0° and 180° for a total of 19 MM simulations. Each butane MM gas phase simulation underwent a short equilibration prior to production simulations. Data collection was done during a 1 ns Langevin dynamics simulation that was propagated with a 1 fs time step and used a friction coefficient of 1 ps^{-1}. During the simulation, coordinates were saved every 10 fs, and coordinate/velocity information was saved every 1 ps.

The final QM level PMF was elucidated via the indirect framework as laid out in Figure S1. Each incremental ΔA^{MM} was computed with BAR using 1.9 million MM snapshots (100 000 per step along the reaction path). Calculation of the $\Delta A^{MM\to QM}$ was performed using both one-sided equilibrium and nonequilibrium methods. First, the standard FEP free energies were generated based on all data collected from the MM ensembles, i.e., computing 1.9 million HF/6-31G* single point energies.[31] Next, the NEW, $W_{MM\to QM}$, was calculated

DOI: 10.1021/acs.jpclett.5b02164
J. Phys. Chem. Lett. 2015, 6, 4850−4856

through a series of 50 step fast switching simulations between MM and HF/6-31G*, starting from the coordinate/velocity information collected during the production MM simulations (1000 fast switching simulations per step along the reaction path), and used to find $\Delta A^{MM\rightarrow QM}$ via JAR.

Both the FEP and the JAR,FW50 standard deviations and hysteresis estimates were generated analogously to Ala/Ser (see above); i.e., via block averaging of 10 sequential subsets of data with blocks of 10 000 and 100 data points for FEP and JAR,FW50, respectively. The reference PMF, from 0° to 180°, used for comparison was generated as described in ref 17, i.e., via FEP between SCC-DFTB (3ob-3−1) and HF/6-31G* using a total of 3.6 million data points. This reference is very well converged as the overlap between SCC-DFTB and HF is nearly perfect for butane.

■ ASSOCIATED CONTENT

Supporting Information

The Supporting Information is available free of charge on the ACS Publications website at DOI: 10.1021/acs.jpclett.5b02164.

Free energy results for the "direct" BAR calculations DFTB to DFTB3 and C22 to C22(CMAP)); figure illustrating the extended thermodynamic cycle used for calculating butane PMFs; and φ, ψ and χ_1 plots for all simulations run (i.e., both equilibrium and nonequilibrium) (PDF)

■ AUTHOR INFORMATION

Corresponding Authors

*E-mail: hlw@usf.edu.

*E-mail: stefan@mdy.univie.ac.at.

Notes

The authors declare no competing financial interest.

■ ACKNOWLEDGMENTS

S.B. thanks Christoph Dellago for insightful discussions concerning nonequilibrium work methods. H.L.W. and P.S.H. would like to thank Ms. Fiona Kearns for helpful discussions. H.L.W. would like to highlight that this material is based upon work supported by the National Science Foundation under CHE-1464946. Further, HLW and PSH thank USF Research Computing (Circe) for their patience and assistance and the NSF for support via their Major Research Instrumentation Program (MRI 1531590).

■ REFERENCES

(1) Gao, J.; Xia, X. A Priori Evaluation of Aqueous Polarization Effects through Monte Carlo QM-MM Simulations. *Science* **1992**, *258*, 631−5.

(2) Gao, J.; Luque, F. J.; Orozco, M. Induced Dipole Moment and Atomic Charges Based on Average Electrostatic Potentials in Aqueous Solution. *J. Chem. Phys.* **1993**, *98*, 2975.

(3) Luzhkov, V.; Warshel, A. Microscopic Models for Quantum Mechanical Calculations of Chemical Processes in Solutions: LD/AMPAC and SCAAS/AMPAC Calculations of Solvation Energies. *J. Comput. Chem.* **1992**, *13*, 199−213.

(4) Wesolowski, T.; Warshel, A. Ab Initio Free Energy Perturbation Calculations of Solvation Free Energy Using the Frozen Density Functional Approach. *J. Phys. Chem.* **1994**, *98*, 5183−5187.

(5) Gao, J.; Freindorf, M. Hybrid ab Initio QM/MM Simulation of N -Methylacetamide in Aqueous Solution. *J. Phys. Chem. A* **1997**, *101*, 3182−3188.

(6) Zheng, Y. J.; Merz, K. M. Mechanism of the Human Carbonic Anhydrase II-Catalyzed Hydration of Carbon Dioxide. *J. Am. Chem. Soc.* **1992**, *114*, 10498−10507.

(7) Zwanzig, R. W. High-Temperature Equation of State by a Perturbation Method. I. Nonpolar Gases. *J. Chem. Phys.* **1954**, *22*, 1420.

(8) Štrajbl, M.; Hong, G.; Warshel, A. Ab Initio QM/MM Simulation with Proper Sampling: "First Principle" Calculations of the Free Energy of the Autodissociation of Water in Aqueous Solution. *J. Phys. Chem. B* **2002**, *106*, 13333−13343.

(9) Rosta, E.; Klähn, M.; Warshel, A. Towards Accurate Ab Initio QM/MM Calculations of Free-Energy Profiles of Enzymatic Reactions. *J. Phys. Chem. B* **2006**, *110*, 2934−2941.

(10) Plotnikov, N. V.; Kamerlin, S. C. L.; Warshel, A. Paradynamics: an Effective and Reliable Model for Ab Initio QM/MM Free-Energy Calculations and Related Tasks. *J. Phys. Chem. B* **2011**, *115*, 7950−7962.

(11) Pohorille, A.; Jarzynski, C.; Chipot, C. Good Practices in Free-Energy Calculations. *J. Phys. Chem. B* **2010**, *114*, 10235−10253.

(12) Heimdal, J.; Ryde, U. Convergence of QM/MM Free-Energy Perturbations Based on Molecular-Mechanics or Semi-Empirical Simulations. *Phys. Chem. Chem. Phys.* **2012**, *14*, 12592−12604.

(13) König, G.; Hudson, P. S.; Boresch, S.; Woodcock, H. L. Multiscale Free Energy Simulations: An Efficient Method for Connecting Classical MD Simulations to QM or QM/MM Free Energies Using Non-Boltzmann Bennett Reweighting Schemes. *J. Chem. Theory Comput.* **2014**, *10*, 1406−1419.

(14) Genheden, S.; Cabedo Martinez, A. I.; Criddle, M. P.; Essex, J. W. Extensive All-Atom Monte Carlo Sampling and QM/MM Corrections in the SAMPL4 Hydration Free Energy Challenge. *J. Comput.-Aided Mol. Des.* **2014**, *28*, 187−200.

(15) Cave-Ayland, C.; Skylaris, C.-K.; Essex, J. W. Direct Validation of the Single Step Classical to Quantum Free Energy Pertubation. *J. Phys. Chem. B* **2015**, *119*, 1017−1025.

(16) König, G.; Brooks, B. R. Correcting for the Free Energy Costs of Bond or Angle Constraints in Molecular Dynamics Simulations. *Biochim. Biophys. Acta, Gen. Subj.* **2015**, *1850*, 932−943.

(17) Hudson, P. S.; White, J. K.; Kearns, F. L.; Hodoscek, M.; Boresch, S.; Woodcock, H. L. Efficiently Computing Pathway Free Energies: New Approaches Based on Chain-of-Replica and Non-Boltzmann Bennett Reweighting Schemes. *Biochim. Biophys. Acta, Gen. Subj.* **2015**, *1850*, 944−953.

(18) Sampson, C.; Fox, T.; Tautermann, C. S.; Woods, C.; Skylaris, C.-K. A "Stepping Stone" Approach for Obtaining Quantum Free Energies of Hydration. *J. Phys. Chem. B* **2015**, *119*, 7030−7040.

(19) Genheden, S.; Ryde, U.; Söderhjelm, P. Binding Affinities by Alchemical Perturbation Using QM/MM with a Large QM System and Polarizable MM Model. *J. Comput. Chem.* **2015**, *36*, 2114−2124.

(20) Bentzien, J.; Muller, R. P.; Florián, J.; Warshel, A. Hybrid ab Initio Quantum Mechanics/Molecular Mechanics Calculations of Free Energy Surfaces for Enzymatic Reactions: The Nucleophilic Attack in Subtilisin. *J. Phys. Chem. B* **1998**, *102*, 2293−2301.

(21) Bennett, C. H. Efficient Estimation of Free Energy Differences from Monte Carlo Data. *J. Comput. Phys.* **1976**, *22*, 245−268.

(22) Jarzynski, C. Nonequilibrium Equality for Free Energy Differences. *Phys. Rev. Lett.* **1997**, *78*, 2690−2693.

(23) Crooks, G. E. Path-Ensemble Averages in Systems Driven Far from Equilibrium. *Phys. Rev. E: Stat. Phys., Plasmas, Fluids, Relat. Interdiscip. Top.* **2000**, *61*, 2361−2366.

(24) Dellago, C.; Hummer, G. Computing Equilibrium Free Energies Using Non-Equilibrium Molecular Dynamics. *Entropy* **2014**, *16*, 41−61.

(25) Mackerell, A. D.; Feig, M.; Brooks, C. L. Extending the Treatment of Backbone Energetics in Protein Force Fields: Limitations of Gas-Phase Quantum Mechanics in Reproducing Protein Conformational Distributions in Molecular Dynamics Simulations. *J. Comput. Chem.* **2004**, *25*, 1400−1415.

(26) Wood, R. H.; Muhlbauer, W. C. F.; Thompson, P. T. Systematic Errors in Free Energy Perturbation Calculations due to a Finite

DOI: 10.1021/acs.jpclett.5b02164
J. Phys. Chem. Lett. 2015, 6, 4850−4856

Sample of Configuration Space: Sample-Size Hysteresis. *J. Phys. Chem.* **1991**, *95*, 6670−6675.
(27) Brooks, B. R.; Brooks, C. L.; Mackerell, A. D.; Nilsson, L.; Petrella, R. J.; Roux, B.; Won, Y.; Archontis, G.; Bartels, C.; Boresch, S.; et al. CHARMM: The Biomolecular Simulation Program. *J. Comput. Chem.* **2009**, *30*, 1545−1614.
(28) Woodcock, H. L.; Miller, B. T.; Hodoscek, M.; Okur, A.; Larkin, J. D.; Ponder, J. W.; Brooks, B. R. MSCALE: A General Utility for Multiscale Modeling. *J. Chem. Theory Comput.* **2011**, *7*, 1208−1219.
(29) Woodcock, H. L.; Hodoscek, M.; Gilbert, A. T. B.; Gill, P. M. W.; Schaefer, H. F.; Brooks, B. R. Interfacing Q-Chem and CHARMM to Perform QM/MM Reaction Path Calculations. *J. Comput. Chem.* **2007**, *28*, 1485−1502.
(30) Riccardi, D.; Cui, Q. pKa Analysis for the Zinc-Bound Water in Human Carbonic Anhydrase II: Benchmark for "Multiscale" QM/MM Simulations and Mechanistic Implications. *J. Phys. Chem. A* **2007**, *111*, 5703−5711.
(31) Shao, Y.; Gan, Z.; Epifanovsky, E.; Gilbert, A. T.; Wormit, M.; Kussmann, J.; Lange, A. W.; Behn, A.; Deng, J.; Feng, X.; et al. Advances in Molecular Quantum Chemistry Contained in the Q-Chem 4 Program Package. *Mol. Phys.* **2015**, *113*, 184−215.
(32) Gordon, M. S.; Schmidt, M. W. In *Theory and Applications of Computational Chemistry: The First Forty Years*; Dykstra, C. E., Frenking, G., Kim, K. S., Scuseria, G. E., Eds.; Elsevier: Amsterdam, 2005; pp 1167−1189.
(33) Guest, M. F.; Bush, I. J.; Van Dam, H. J. J.; Sherwood, P.; Thomas, J. M. H.; Van Lenthe, J. H.; Havenith, R. W. A.; Kendrick, J. The GAMESS-UK Electronic Structure Package: Algorithms, Developments and Applications. *Mol. Phys.* **2005**, *103*, 719−747.
(34) Vanommeslaeghe, K.; Hatcher, E.; Acharya, C.; Kundu, S.; Zhong, S.; Shim, J.; Darian, E.; Guvench, O.; Lopes, P.; Vorobyov, I.; et al. CHARMM General Force Field: A Force Field for Drug-Like Molecules Compatible with the CHARMM All-Atom Additive Biological Force Fields. *J. Comput. Chem.* **2010**, *31*, 671−690.

DOI: 10.1021/acs.jpclett.5b02164
J. Phys. Chem. Lett. 2015, 6, 4850−4856